PAPER

On the nature of droplet production in DC glows with a liquid anode: mechanisms and potential applications

To cite this article: Zimu Yang et al 2022 Plasma Sources Sci. Technol. 31 115008

View the article online for updates and enhancements.

You may also like

- What Are the Effective Reactants in the Plasma-Induced Wastewater Treatment? Bangbang He, Xinning Gong, Xin Wang et al
- Quantification of plasma produced OH and electron fluxes at the liquid anode and their role in plasma driven solution electrochemistry

Yuanfu Yue, Stephen Exarhos, Jaehyun Nam et al

 A review of plasma-liquid interactions for nanomaterial synthesis
 Qiang Chen, Junshuai Li and Yongfeng Li



Plasma Sources Sci. Technol. 31 (2022) 115008 (10pp)

https://doi.org/10.1088/1361-6595/ac9c8e

On the nature of droplet production in DC glows with a liquid anode: mechanisms and potential applications

Zimu Yang¹, Yao Kovach¹, Zhehui Wang² and John Foster^{1,*}

E-mail: jefoster@umich.edu

Received 5 September 2022 Accepted for publication 21 October 2022 Published 9 November 2022



Abstract

The interactions between plasma and liquid solutions give rise to the formation of chemically reactive species useful for many applications, but the mass transport in the interfacial region is usually limited and not fully understood. In this work, we report on the observation and explanation of droplet ejection at the plasma-liquid interface of a one-atmosphere glow discharge with the liquid anode. The impact of droplets emission on plasma properties is also analyzed by spectroscopy. The process, which is an efficient mass and charge transport mechanism, apparently occurs during discharge operation and thus constitutes a feedback vehicle between the discharge and the liquid. Distinctive from the well-known Talyor cone droplets associated with liquid cathodes, the observed droplets originate from the bubbles due to electrolysis and solvated air which does not require strong electric field at liquid surface. Instead, the droplets are ejected by bubble cavity rupture at the plasma-liquid interface and their size, initial speed are strongly dependent on the gravity, inertia and capillarity. The droplets emerge near the plasma attachment and are subsequently vaporized, emitting intense UV and visible light, which originated from excited OH radicals and sodium derived from the liquid electrolyte. Spectroscopy analysis confirmed that the bursting droplets generally reduce the gas temperature while their effects on electron density depend on the composition of the liquid anode. Results also show that droplets from NaCl solution increase the plasma electron density due to the lower ionization potential of sodium. These findings reveal a new mechanism for discharge maintenance and mass transport as well as suggest a simple approach to dispersing plasma-activated liquid into the gas phase and thus enhancing plasma-liquid interaction.

Keywords: plasma-liquid interactions, interfacial mass transfer, plasma-aerosol, optical emission spectroscopy

Supplementary material for this article is available online

(Some figures may appear in colour only in the online journal)

0963-0252/22/115008+10\$33.00

© 2022 IOP Publishing Ltd Printed in the UK

¹ Plasma Science and Technology Laboratory, Dept. Nuclear Engineering and Radiological Sciences, University of Michigan, Ann Arbor, MI 48109, United States of America

² Los Alamos National Lab, Los Alamos, NM 87545, United States of America

^{*} Author to whom any correspondence should be addressed.

1. Introduction

A non-thermal plasma interacting with liquid solution produces a host of reactive species: oxygen atom, OH radical, hydrogen peroxide, and UV light [1]. These species can be utilized in applications ranging from water treatment to medicine. Our understanding of processes prevailing at the plasma-liquid interface however remains incomplete. Contributing to the complexity of plasma-liquid interface are the coupling processes where thermodynamics and mass transport phenomena are correlated in the chemically reactive multiphase media [2]. Based on a pin-to-water-surface discharge configuration, adding aerosols to the plasma can greatly expand the surface-to-volume ratio which enhances the transfer of activation energy from the plasma to the liquid, delivery of short-lived species, and controlling reactivity in the liquid [3]. The generation mechanisms of aerosols usually include evaporation, surface deformation, and external source such as electrospray. Strong mist containing particles from cathodic electrolytes are reported [4, 5]. Prominent surface deformation and aerosols from Taylor cone are only found in cathodic electrolytes [5–7] while the anodic liquid surface features a relatively unperturbed surface where the plasma attachment can self-organize into intricate patterns [8] accompanied by convective flow driven by heat [9]. As reported in the literature [6], the anode fall voltage drop and liquid sheath electric field at the anodic electrolyte are too weak to trigger a Taylor cone deformation. In our previous research, the emission phenomenon of particles from molten droplets originating from the FeCl₃ liquid anode solution is reported but the detailed formation mechanism is unclear [10]. To unfold this mystery, we utilize high-speed camera imaging to study the droplet ejection directly. Statistically, the droplets of $40-120 \mu m$ in diameter are ejected by a liquid jet at speeds up to 9 m s⁻¹. Analysis shows these are jet droplets formed when the bubble cavity collapses at gas-liquid interface and forms a vertical upward jet that pinch off into droplets. The bubbles can either be dissolved air released by plasma gas heating or oxygen from electrolysis. A similar phenomenon can also be found in a melted liquid wall of tokamak plasma [11]. The jet droplets process indeed is ubiquitous and well known in the mass transport of sea aerosol into the atmosphere [12, 13]. Interestingly the process also leads to uptake of atmospheric gas by the liquid as well. In this regard, the process may be an important two-way mass transport mechanism.

After ejection into the nonthermal plasma, the small droplets are subject to a variety of forces including electrostatic forces due to droplet charging, thermophoresis, and gas dynamic drag force associated with convection. These forces along with gravity determine not only the motion of the droplets but also their duration of the interaction. Polarization effects driven by the electric fields as well as simple charge collection can lead to disruption, resulting in the production of even smaller droplets. A nonthermal plasma consists of an active zone associated with the ionization wave and the corona or afterglow region where droplets can deform and vaporize by the forces and thermal energy exchange. Such evaporation

changes the size of the particles which in turn changes the magnitude of forces acting on the particle as well. The mass transport of species from the water into the discharge not only augments the gas-phase chemistry by providing a source of new reactants but also affects discharge impedance through cooling and the introduction of the charge and nanoparticles. Indeed, droplets may play an important role in charge transport between phases. The species introduced by the droplets can be quite complex especially if they are synthesized in solution such as glow discharge electrolytic cells with liquid anode or cathode electrode [14]. Droplets derived from these solutions can contain nanoparticles that ultimately interact with the gas phase plasma offering new opportunities for nonequilibrium processing as they transit the nonthermal plasma. This process can be used potentially for applications ranging from decontamination and agriculture to material processing [15].

This work however focuses on the mechanism of droplet formation and the preliminary diagnostics of its impact on plasma properties via spectroscopy. Experiments described herein demonstrate that the source of the droplets is gas bubbles that upon breaking the surface generate a high-speed jet at the interface. These bubbles contain species produced within the liquid phase and thus are a mechanism for mass transport into the gas phase—such as metal ions and even nanoparticles. Optical spectroscopy is also used to reveal the droplet composition and its impact on plasma properties. This new mass transport mechanism suggests that material in the liquid can be processed by the plasma there thus providing a new approach to material processing and chemical synthesis.

2. Experimental method

Figure 1 illustrates the DC liquid anode discharge setup, which is similar to that used in our previous work [8, 16]. The discharge apparatus consisted of a brass tube cathode with a 500 μ m channel for gas flow. A continuous helium flow up to 200 sccm was used to stabilize the discharge from thermalization. A glow discharge plasma could be formed by a 3 kV DC power supply between the brass electrode and a liquid electrolyte through the application of high voltage DC. A shunt resistor combined with a voltage multimeter and high voltage probe Tektronix P6015A were used to monitor the discharge current and voltage, respectively. A series resistor of 15.73 $k\Omega$ was used to ballast the discharge current. A stepper motor was used to adjust the electrode-surface gap. The nominal discharge gap was 8 mm. The external circuit and typical current-voltage curve response for a range of electrolytes were described in detail elsewhere [8]. It is noted that the droplet ejection process is a fluid dynamics phenomenon driven by heat transfer and electrolysis which is not unique in this discharge configuration. Furthermore, the ejection of droplets and their emission near plasma was found to be highly random and discontinuous which makes the acquisition of emission spectra time-consuming. This might explain the paucity of published data on droplet formation with liquid anode systems.

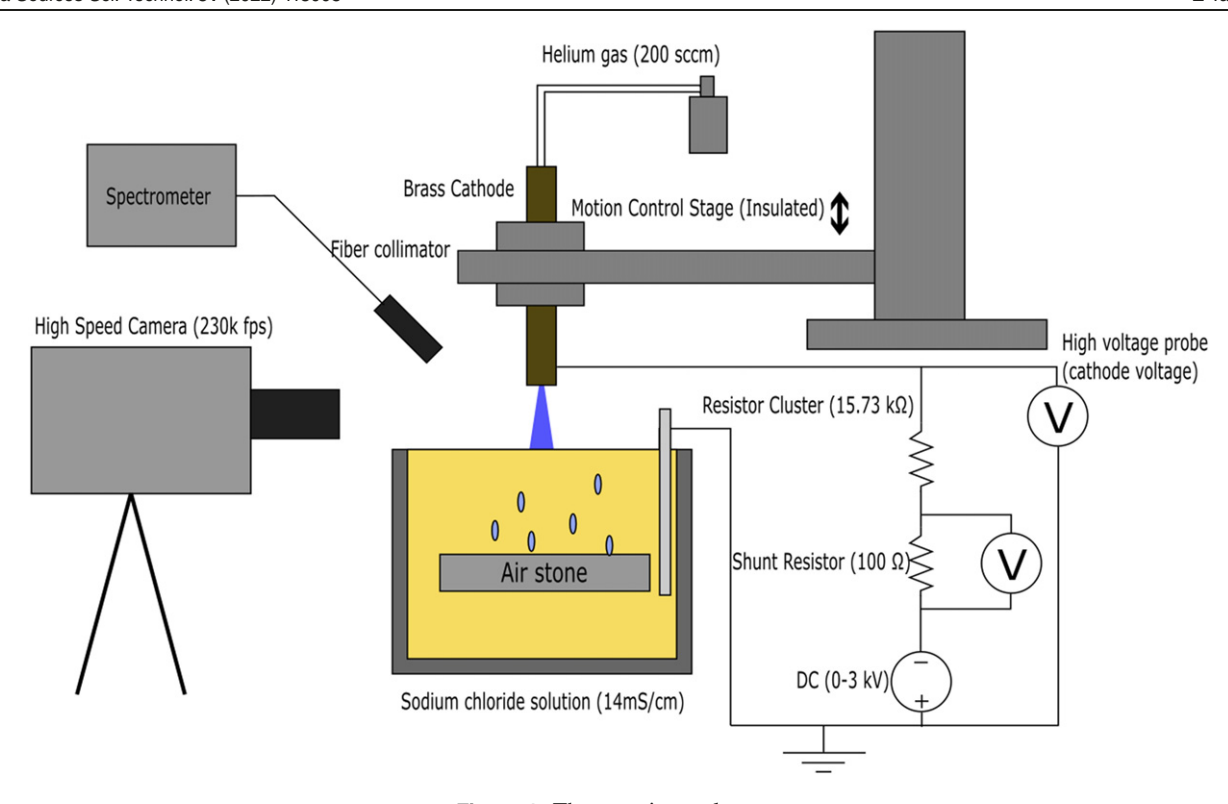


Figure 1. The experimental setup.

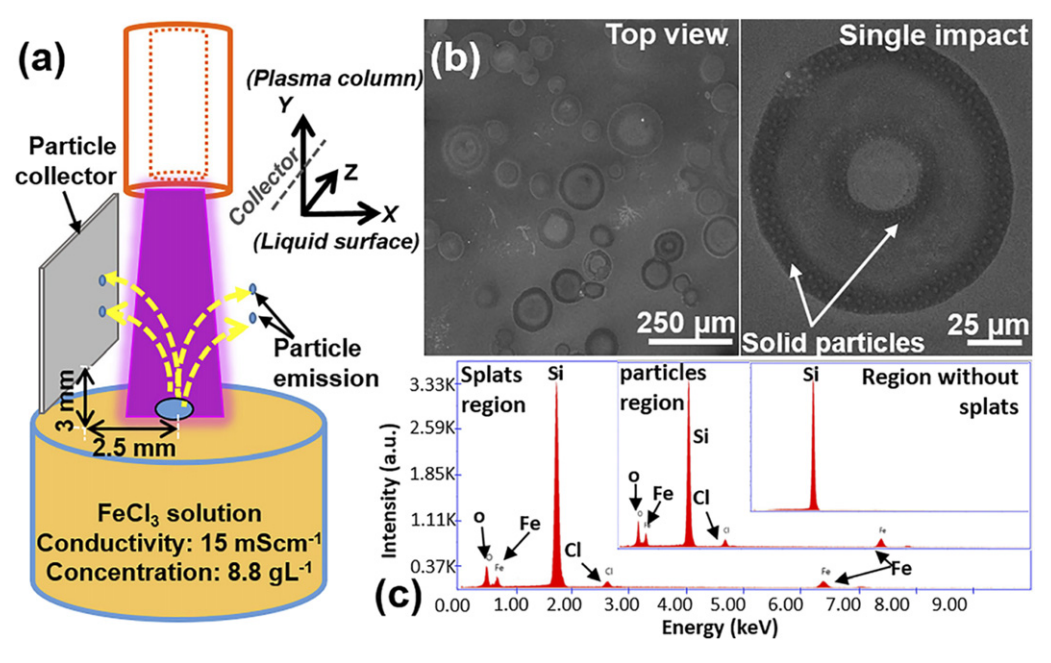


Figure 2. Schematic of particle collection setup is shown in (a), scanning electron microscopy images of the resulting splats after the collection in (b), and (c) the composition spectrum detected using energy dispersive x-ray analysis from various regions. Reprinted from [10], with the permission of AIP Publishing.

After identifying the presence of this natural droplet emission process, to better understand the nature of droplet interaction with the gas phase plasma, an air sparger was introduced to generate a stream of bubbles for the ejection of droplets via rupturing process. In this work, an aquarium air stone was placed underneath the liquid surface to produce gas bubbles in an attempt to boost and control the droplet ejection via

bubble rupturing near the interface. This experimental approach poses a new method to enhance mass transport into the plasma through the production of aerosol at the interface. Different liquid electrolytes including deionized water (44 μ S cm⁻¹), NaCl (14 mS cm⁻¹), FeCl₃ (12 mS cm⁻¹), and CuSO₄ (15 mS cm⁻¹) solutions were used to study the plasma response to the droplets.

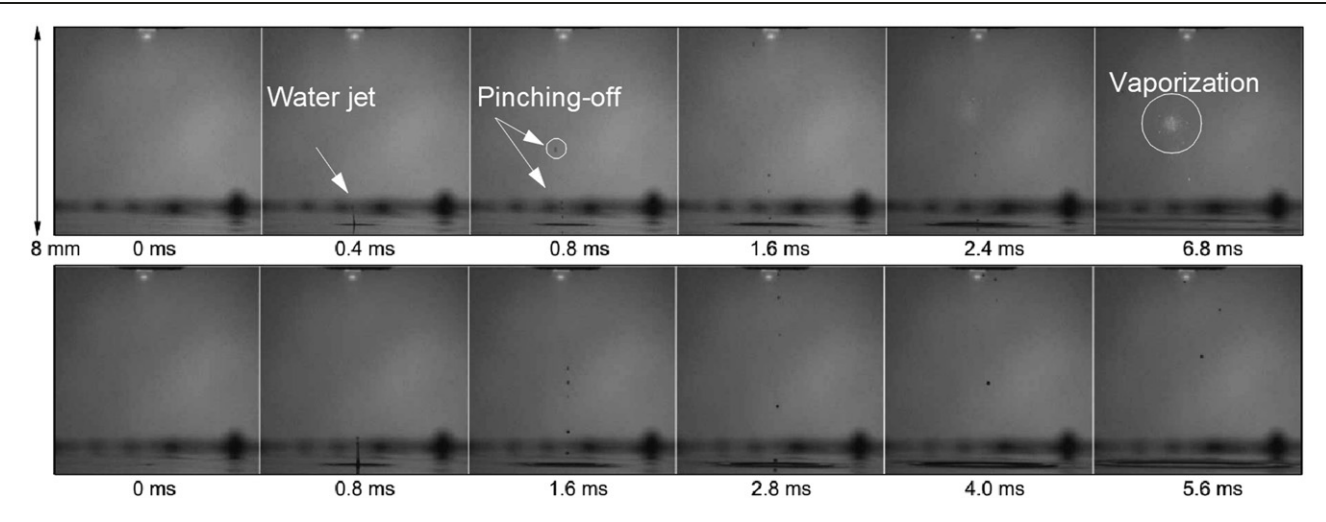


Figure 3. The droplet ejection under DC discharge. Droplets have an average speed of 3 m s⁻¹ and a diameter of 85 μ m. Supplementary file Clip1.mp4 is available to show the corresponding video. (FeCl₃ solution, 90 mA discharge current, film speed 12.5 k fps).

To capture the trajectory of droplets burst, a high-speed camera (Phantom TMX 7510) coupled with a macro lens is used to record the events at up to 230 k fps and 8 × 8 mm field of view. Additionally, a fast medium-wave infrared camera (FLIR X8500sc) was used to measure the thermal signature of the droplets. The open-source video analysis tool Tracker [17] was used to study the motion of droplets. The optical emission from the plasma and its interaction with droplets is captured using a Czerny–Turner type spectrometer (Acton Series, SP-2300i) with an 1800-grooves/mm holographic grating and a fast intensified CCD detector (PI-MAX3, Princeton Instruments). Optical emission from the mid-region of the positive column was collected using an optical fiber. This region was imaged because it was found from analysis of fast camera data that the droplets most frequently burst there.

3. Results and discussion

3.1. Observation of droplet ejection

As has been shown by Bruggeman [6], Shirai [5], the liquid anode surface electric field is too weak to generate droplets via the Taylor cone mechanism. However, our previous research revealed that this surface is active, with the emission of many particles from the FeCl₃ liquid anode [10]. As shown in figure 2, the composition of these particles was found to be identical to the nanoparticles generated in the electrolytic solution. At the time of that study, it was not known how these particles were emitted into the plasma. This present work provides very strong evidence that the delivery mechanism of the particles was droplet production via bubble rupture at the interface and thus suggests an important mechanism for mass transport. Figure 3 shows two typical examples of droplet ejection events captured at the speed of 12.5 k fps. Supplementary file Clip1.mp4 is available to show the corresponding video. See supplementary file Clip2.mp4 for showing the bubble rupture and droplets formation at a different angle. The liquid anode is FeCl₃ with a conductivity of 12 mS cm⁻¹. The generation of droplets usually starts with a rising jet which is then pinched off into a chain of droplets by an end pinching process [18]. The top droplet at the jet tip usually has the highest velocity ranges from 1–9 m s⁻¹. The process itself is indeed classic droplet jet formation.

Compared to the Taylor cone droplets from the liquid cathode, the magnitude of aerosol flux formed at the liquid anode is largely dependent on the nature of the dissolved gas source with droplet average velocity being relatively independent of the magnitude of the local applied electric field. Another significant variance is in the fluid dynamics where the observed droplet is ejected vertically via a water jet while Taylor cone droplets are formed in large amounts and all directions at once. It is expected that as the droplets traverse the discharge, surface evaporation will lead to the introduction of liquidderived species into the gas phase. Complete evaporation or rapid disruption is also possible during droplet transit. Indeed, droplet disruption in the gas phase can only happen if its size is small enough or the velocity is slow enough so that the droplets can completely evaporate. As shown in figure 3, the progeny droplet in the first example (51 μ m) is smaller than the example in the second row (90 μ m) which did not vaporize. Other cases show the survival of droplets at a size of only 40 μ m but having a speed of 8 m s⁻¹. As for the other electrolytes, we also observe the droplet ejection from DI water and NaCl solution as the liquid anode. According to high-speed camera imaging, the rate of droplet ejection does not depend on the type of electrolytes, while solutes such as Fe³⁺ and Na⁺ make the droplet ejection observable to the eyes due to its bright emission upon vaporization. On the other hand, DI water droplets emission is difficult to detect owing to the absence of species that emit at wavelengths other than that associated with water, which is ubiquitous in the discharge. The sensitivities of droplet emission to parameters such as conductivity, pH, and plasma chemistry are not explored in this

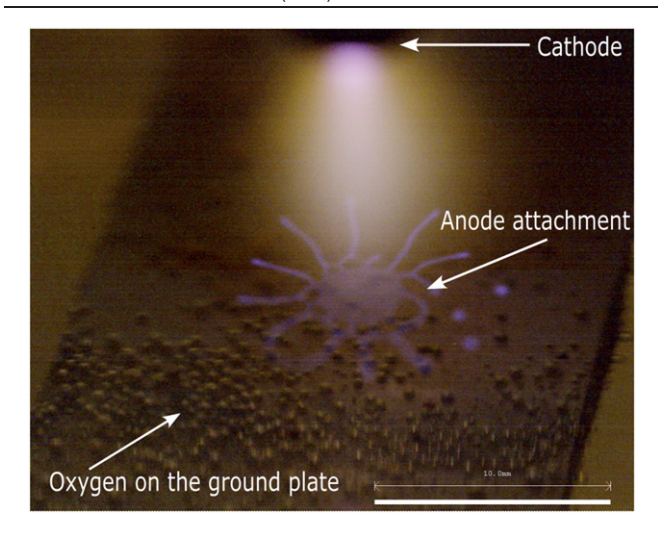


Figure 4. Gas bubbles due to electrolysis at the submerged anode (anode is a silicon plate).

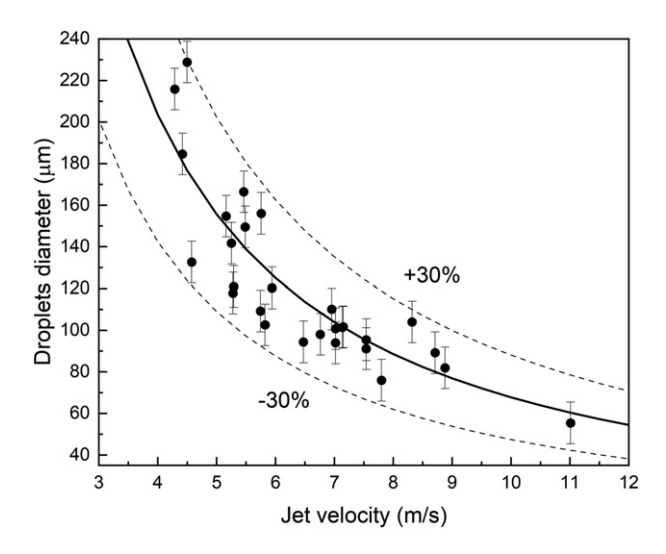


Figure 5. Jet droplets diameter vs jet velocity. The solid curve represents the theoretical scaling law [27] and the dots with the error bar show experiment results from this work. (Density 977 kg m⁻³, surface tension 64.4 mN m⁻¹, water surface temperature 70 °C.)

3.2. The mechanism of droplets formation

As discussed and inferred from experimental observations, the mechanism for droplet emission in this work via bubble rupture at the interface is compelling. Another possible mechanism related to electrohydrodynamic (EHD) instability should also be briefly discussed. Recently, linear perturbation analysis of the plasma–liquid interface including the sheath electric field on the EHD instability was performed [19]. For an atmospheric pressure plasma that has an electron temperature of 5 eV and density of 10^{14} cm⁻³, the resulting critical surface potential is 3 kV for EHD instability including the ion impact. This value is even higher than the discharge voltage, therefore the EHD instability alone could not cause the formation of droplets.

Since bubbles are observed to drive the droplet ejection (see supplementary file Clip2.mp4), their origin is also critical. There are two major sources of bubbles in the liquid phase.

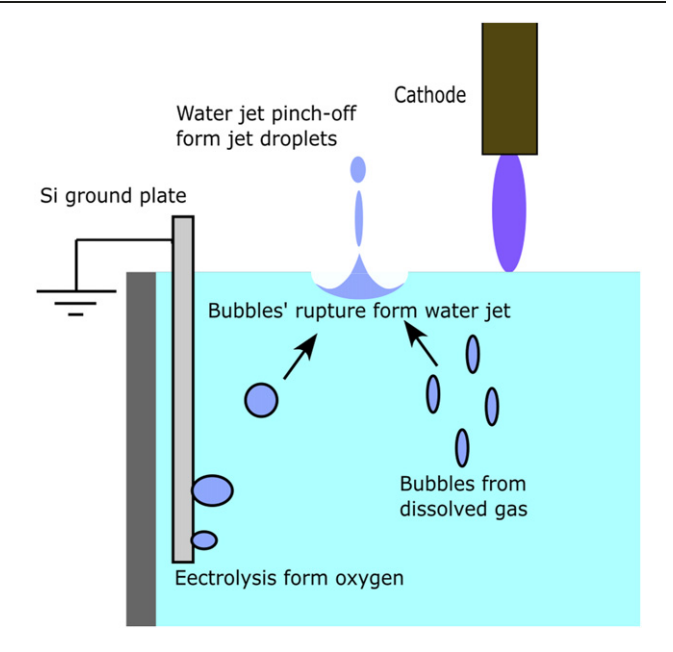


Figure 6. Schematic of droplets emission mechanism.

The first source is the solvated air in the liquid phase whose solubility decreases when the temperature is raised as the liquid is heated by the discharge. In fact, this explains why the droplet ejection is highly random and not readily apparent instantaneously after the plasma ignition—the liquid needs time to heat up thoroughly. In a tokamak, the trapped gas in the melting wall surface can also form the jet and bursting droplets [11]. In further support of the dissolved gas theory, the liquid anode solution is degassed by boiling and results show that the droplet ejection is significantly reduced but still exists suggesting incomplete degassing or that another gas source must be present. The immersed anode is another gas source that has to be accounted for. Oxidation of water at the anode gives rise to the production of oxygen gas bubbles as shown in figure 4. These gas bubbles can also detach, rise, and rupture at the interface, forming droplets. However, the anode plate is usually placed away from the plasma attachment so that this source is not dominant. At the plasma-liquid interface, many researchers also show that hydrogen can be generated through the reduction of protons by plasma electrons [20–22]. It is unknown whether the hydrogen gas could form gas bubbles at the surface since the solvated electrons can only exist under the interface around 12.3 nm [23]. A detailed measurement of the gas bubble's composition will need to be conducted in the future. In any case, bubbles are clearly present from many sources in these discharges.

When a gas bubble reaches a free liquid surface, its upper surface will protrude from the liquid—air interface, drain, and ruptures due to the gravitational force [24]. The shattering of the cavity and capillarity forms a central jet which then breaks up into soaring droplets from the pinching-off process [25]. The radius of these droplets ranges from 2 to 500 μ m and is related to the size of the bubble [26]. Such a phenomenon can be observed in diverse settings ranging from effervescent beer to vast ocean surface.

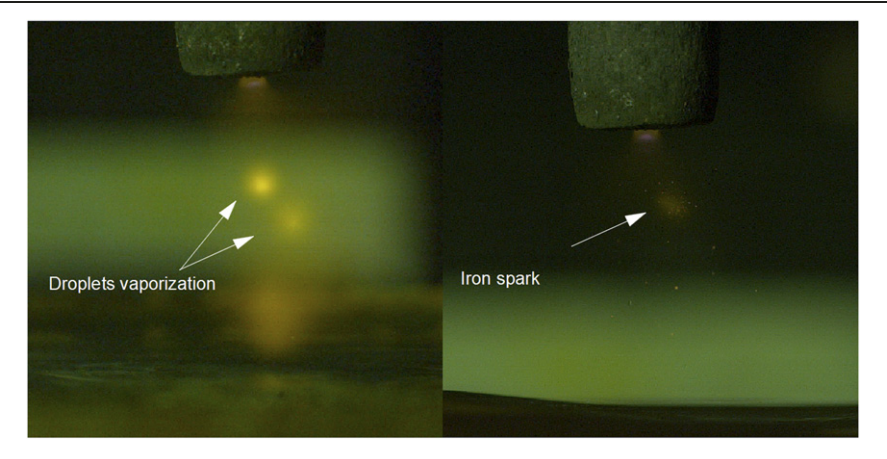


Figure 7. Evaporation of droplets and their subsequent optical emissions in the plasma. Note the differences in emission color. (Left: NaCl solution, right: FeCl₃ solution.)

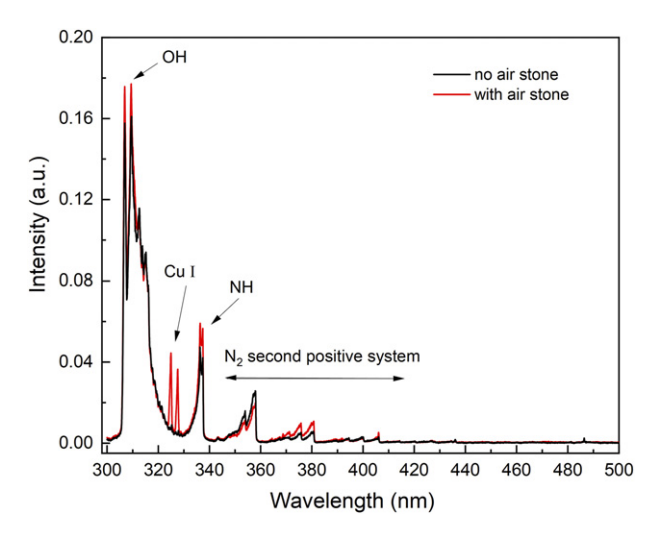


Figure 8. Optical emission spectra using a CuSO₄ liquid anode (discharge current: 80 mA, liquid anode CuSO₄ solution with initial conductivity: 15 mS cm⁻¹).

It has been shown that the first droplet formed from endpinching at the tip of the jet scales with the radius of the bubble [12]. However, this scaling law contains both the jet formation and droplet detaching processes, coupling the processes together. A recent study further showed that this scaling law can be decoupled from the bubble radius by introducing the jet velocities as the function of the bubble radius [27]. The resulting expression is:

$$Bo_{d} = \frac{\rho g R_{d}^{2}}{\gamma} = 3.55 (Fr_{d}We_{d})^{-3/5}$$

$$= 3.55 \left(\frac{v^{2}}{gR_{d}} \frac{\rho v^{2}R_{d}}{\gamma}\right)^{-3/5}$$
(1)

where ρ , g, γ , R_d , v represent liquid density, acceleration of gravity, surface tension, droplet radius, and initial jet velocity respectively; dimensionless parameters Bond number Bo_d (ratio of gravity to surface tension), Froude number Fr_d (ratio of fluid inertia to gravity), Weber number We_d (ratio of fluid inertia to surface tension) represent the ratio of different

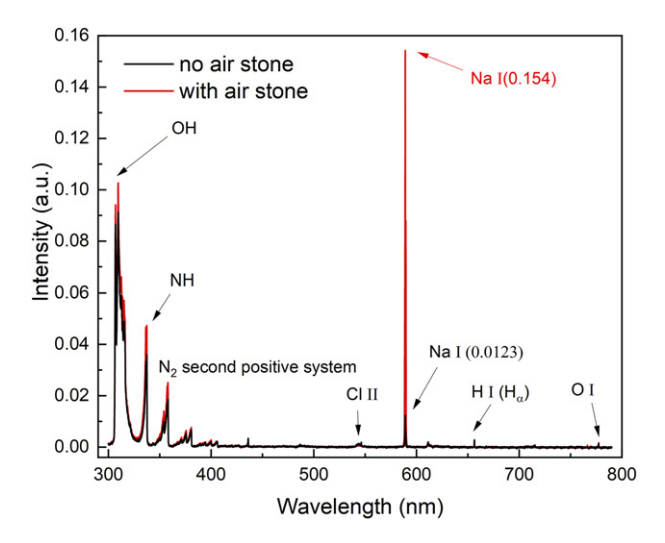


Figure 9. Optical emission spectra using a NaCl liquid anode (discharge current: 50 mA, liquid anode NaCl solution with initial conductivity: 14 mS cm⁻¹).

dynamic forces. Equation (1) can be simplified to:

$$R_{\rm d} = 3.55^{0.5} v^{-1.2} \rho^{-0.2} \gamma^{0.8}. \tag{2}$$

Figure 5 plots the experimental results and theoretical curve based on equation (2) and most of the data fit within this scaling law within 30%. Thus the bursting droplets most likely come from a bubble rupture and water jet pinch-off.

A schematic drawing is shown in figure 6 to illustrate the sequence of bubbles formation, rupture at surface, water jet initiation, and pinch-off into droplets. The whole process is driven by dissolved gas releasing and electrolysis originating from the positive column gas heating and charge transport at the anode while the consequent bubble rupture and droplet ejection are fluid dynamics phenomenon that is not unique in this discharge configuration. Although it is not directly dependent on the discharge, the droplets can work as a vehicle to carry the solute and solvent across the interface and its formation mechanism suggested that it may be

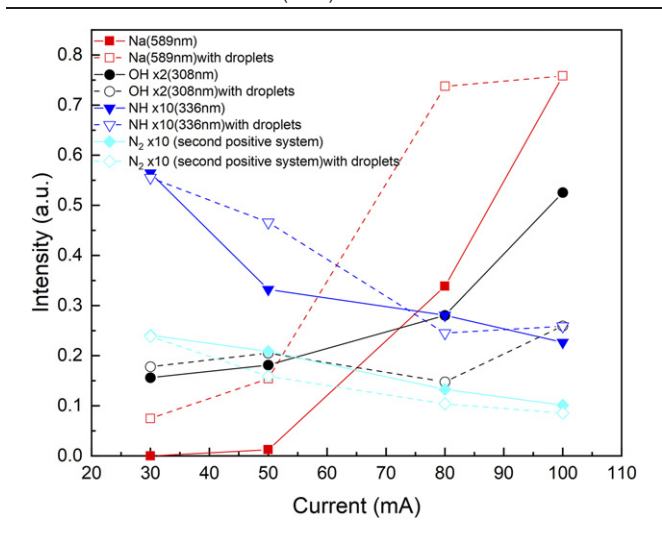


Figure 10. Excited species in plasma using a NaCl liquid anode (liquid anode NaCl solution with initial conductivity: 14 mS cm⁻¹, some species' intensities are adjusted to fit the scale).

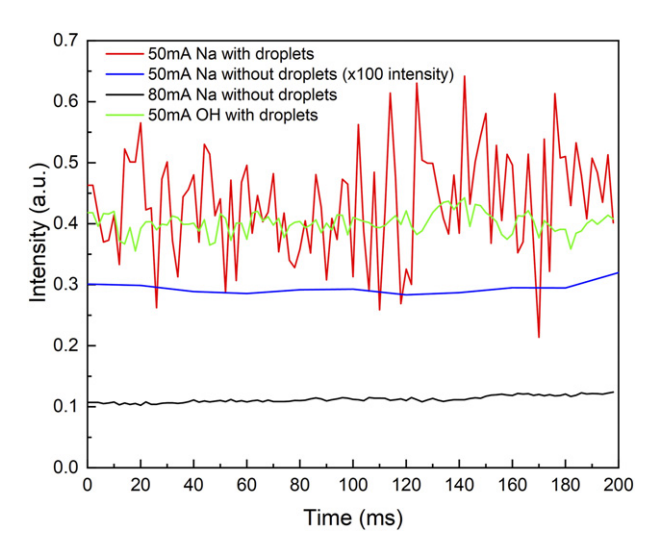


Figure 11. Emission line intensity as a function of time (liquid anode: NaCl solution with initial conductivity: 14 mS cm⁻¹).

feasible to enhance its generation by controlling the rate of bubbles formed in the plasma-activated electrolyte. In this work, we find that droplet ejection is highly random and discontinuous due to the uncontrollable nature of gas bubbles. It is then reasonable and justified to utilize external gas to increase the droplet ejection rate where the mechanism stays the same. As mentioned earlier, a given droplet will tend to evaporate and emit particles only if its speed or volume is small enough. This leads to the need of having fine bubbles (diameter $< 100 \mu m$) since the droplet's diameter is highly dependent on the diameter of the bubble. Figure 7 shows fine droplet ejection and subsequent excitation of species contained within the droplet. These droplets were generated through bubble formation driven by gas injection through the air stone under the liquid anode. It also demonstrates a new method to enhance mass transport at the plasma-liquid interface.

3.3. Droplets emission species analysis by spectroscopy

To study the composition of the droplets in a controlled manner, the air stone sparger was used to generate bubbles that burst at the interface thereby multiplying the droplet formation process. Some fraction of the generated droplets that pass through the plasma column will burst and generate intense optical emissions. The composition of the droplets is then inferred through optical emission spectroscopy. To distinguish the droplet emission from the plasma background emission, we compared the spectrum associated with the plasma at various discharge currents with and without droplet evaporation. Figure 8 shows the spectrum of DC discharge with a CuSO₄ liquid anode electrolyte. The most prominent change observed to occur with droplet emission is the appearance of Cu I (324.8 nm and 327.4 nm) emission lines. Similarly as observed with the sodium chloride solution, droplet emission gave rise to a 12-fold increase in emission intensity of the Na I over the baseline, unperturbed plasma as shown in figure 9. A similar enhancement was also found in FeCl₃ solutions but the scale is much lower. Such relative intensity differences in the observation with various salts can be attributed to variance in oscillator strength f_{ik} and upper energy level E_k magnitude. As can be seen here, ejecting droplets toward the gas phase is an efficient way of adding salt ions, molecules, and nanoparticles from the liquid solution.

Figure 10 shows the relative excited species' emission intensities derived from a NaCl anode electrolyte. The hydroxyl radical species OH (307 nm and 309 nm) increases with current since the higher power provides a higher water evaporation rate and electron density. It should be pointed out that the additional droplets ejection tend to decrease the OH (A) emission at the high current. This reduction is possibly due to the electron temperature drop and a significant reduction in the OH (A) lifetime due to collisional quenching by water molecules [28]. Bruggeman et al [29] show that the density of ground state OH (X) density can be proportional to the square root of water vapor concentration and its spatial profile is broader than the discharge region [30]. The emission of N₂ second positive system and the NH (336 nm) from the reaction between ambient nitrogen and water vapor show a downward trend due to a reduced air fraction in the plasma. Remarkably, the sodium (589 nm) is prominently enhanced by the additional droplets from the air stone. Such effect is very significant at the low current where the sodium emission is extremely low due to the slow mass transport at the plasma-liquid interface. By mechanically ejecting droplets with various salt, the plasma excited species can be changed without adjusting the discharge properties. Another feature of droplet ejection is the time evolution of electrolyte emission as shown in figure 11. The intensity fluctuations last for a millisecond, similar to the time gap between launch and subsequent droplets burst according to the high-speed camera images. In comparison, the other strong emissions from species such as OH, NH feature a smaller magnitude (<11%) of change. We assume that each droplet burst can provide a pulsing dose of electrolyte into the gas phase and thus modify the natural concentration of such

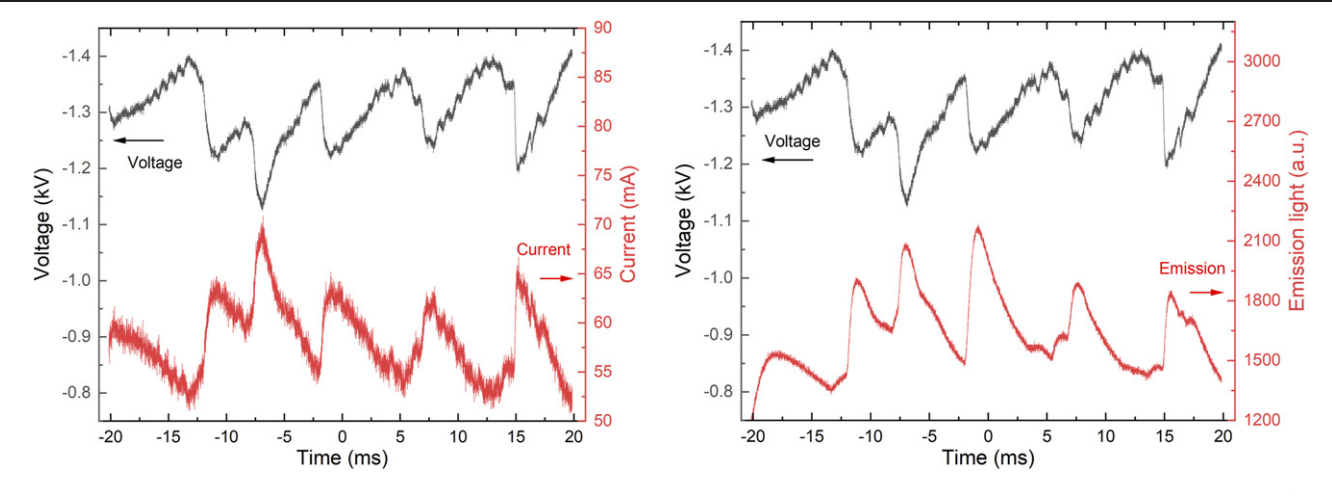


Figure 12. Waveform of DC discharge with droplets burst at 50 mA (liquid anode: NaCl solution with initial conductivity: 14 mS cm⁻¹) left: voltage and current; right: voltage and bulk emission intensity measured by a photodiode.

ions within plasma substantially. A more quantitative model of plasma-chemistry is needed for further understanding of this result.

3.4. Droplets influence on plasma properties

As discussed in the previous subsection, it is expected that the transport of electrolyte species and other particles into the discharge should give rise to overall changes in discharge impedance, particularly at high droplet flux. Indeed, figure 12 shows the modulation in the discharge current, discharge voltage, and discharge light emission (as inferred from a photodiode) with time. The time intervals among these peaks are in milliseconds which again coincides with the droplet ejection period. In the case of no droplets added, we also observe the minor magnitude change of the current-voltage waveform at \sim 10 Hz and it is mainly from the small water level fluctuations due to the capillary wave motion near the plasma attachment. A photodiode that captures the time-resolved emission light intensity indicates a pulsed signal that synchronize with the current-voltage waveforms. If surface deformation is important, the voltage spike should happen before the photodiode signal change since the emission comes from evaporation which happen after the droplet ejection. This leads to the conclusion that those peaks are induced by gas-phase droplet evaporation and species interaction. For a weakly ionized and non-equilibrium plasma, its conductivity mostly depends on the electron mobility and density which gives $\sigma = \frac{n_e e^2}{m \nu_{en}}$. A sudden increase in plasma conductivity means the electron density has risen, or a reduction in the neutral-electron collision frequency. To examine gas-phase plasma properties, we have also investigated changes in gas temperature and electron density by using emission spectroscopy.

The rotational relaxation is a fast process at atmospheric pressure which allows one to estimate the gas temperature from the rotational temperature. Experimentally measured emission spectra from the N_2 second positive system $(N_2:C^3\Pi_u\to B^3\Pi_g)$ is compared with synthetically produced spectra in the range 325–400 nm to determine gas temperature using SPECAIR [31]. Compared to the OH (A-X) spectra,

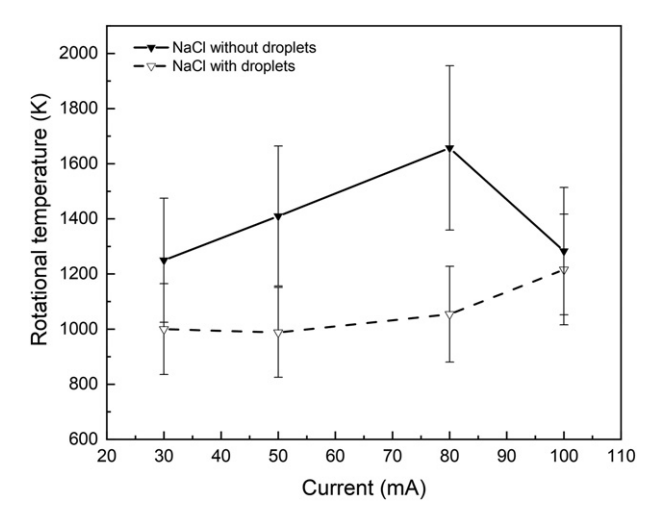


Figure 13. Rotational temperature at various conditions (liquid anode NaCl solution initial conductivity: 14 mS cm⁻¹).

the N_2 second positive system is less sensitive to the water molecule quenching effect. Figure 13 shows the estimated rotational temperature of the plasma with and without droplet ejection. As the discharge current increases monotonically up to approximately 80 mA, above which there is a noticeable drop in temperature. The measured temperature behavior may be an indication that there is a competition between gas heating associated with dissipation in the discharge, which increases with discharge current, and the rate of water evaporation, which also increases with the discharge current. At a fixed current, the additional water vapor from the vaporized droplets cools down the gas temperature in all cases. The data also suggest that, at the highest current, the evaporation rate is comparable to the water introduced by droplets.

Next, the electron density is calculated from the Stark broadening of H_{β} (486.13 nm) Balmer transition due to its large linear Stark effect and bigger full width at half maximum compared to the H_{α} line. Major broadening contributions including instrumental broadening from the spectrometer, Doppler broadening affected by the gas temperature,

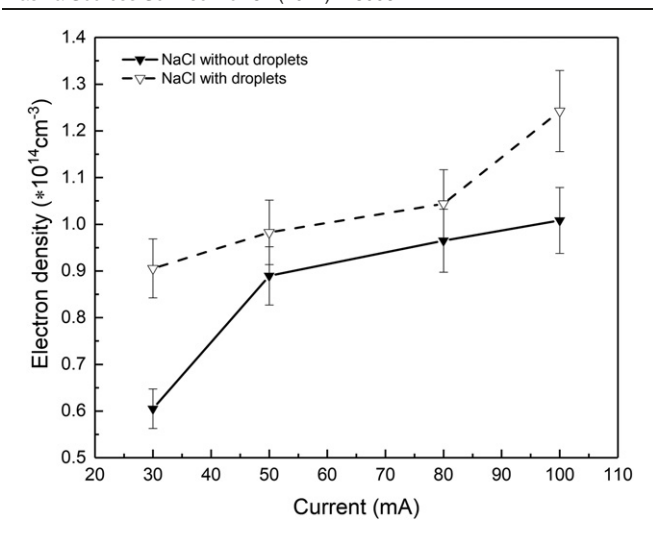


Figure 14. Electron density at various discharge conditions (liquid anode NaCl solution initial conductivity: 14 mS cm⁻¹).

and van der Waals broadening [32] due to collisions among excited hydrogen, water molecule, and air molecules are all considered in the deconvolution procedure for estimation of Stark broadening [33]. For details, the reader is referred to our previous work [8]. As can be seen in figure 14 electron density increases monotonically with discharge current. It is also found that with NaCl electrolyte droplets, the electron density increases suggesting that the low ionization potential sodium atoms derived from evaporating droplets are enhancing the plasma density and offsetting expected losses due to the increased water vapor density. Noted that the spectrometer exposure time is relatively long during which multiple droplets have evaporated and released their emission. In that case, the density change may be transient and its sudden increase causes the plasma conductivity to change abruptly and gives the dynamics shown in figure 12 electrical waveform.

4. Conclusions

In this study, we identify a new mass transport mechanism present in DC glows with liquid anodes—droplet emission. Distinctive from the Taylor cone droplets generated in the liquid cathode, the droplets from the anodic electrolyte surface are produced by a liquid jet that originates from the gas bubbles' rupture at the plasma-liquid interface. The process is ubiquitous in many systems including sea spray generation. It is not inherently a plasma process but the driving forces are provided by the discharge. Specifically, the electrolytic processes at the submerged electrode and heat deposition give rise to the evolution of gas bubbles formed in the liquid solution. The scaling of the liquid jet speed with droplet diameters was found to be consistent with the jet droplet mechanism. Near the plasma column, the jet droplets vaporize and emit intense UV and visible light. To study the transfer process in a more controlled fashion, an air sparger could be used to artificially introduce fine bubbles into the liquid which subsequently formed droplets due to rupture in accordance with the jet droplets mechanism. Optical spectroscopy confirmed that these emissions are from salt particles in the electrolyte and excited OH radicals from the water molecule dissociation. From the current–voltage waveforms, the ejected droplets and the associated salt particles were found to decrease the plasma resistance in a pulsing, intermittent fashion associated with the evaporation and subsequent disruption of a discrete number of bubbles at different times. Further analysis of the emission spectra revealed that the released sodium particles from NaCl liquid anode can increase the electron density due to its low ionization potential. Overall, these findings substantiate a new approach to the mass transfer from the liquid and control of discharge maintenance by dispersing plasma-activated liquid into the gas phase and chemically and ionically enriching the plasma–liquid interaction.

Acknowledgments

This work is supported by the National Science Foundation ECLIPSE program Award No. 2206039, the U.S. Department of Energy, Office of Fusion Energy Sciences, Grant DE-SC0018058. We also acknowledge logistics support made possible via the Department of Energy Contract No. 89233218CNA000001.

Data availability statement

The data that support the findings of this study are available upon reasonable request from the authors.

ORCID iDs

Zimu Yang https://orcid.org/0000-0003-4043-8413
Yao Kovach https://orcid.org/0000-0001-9393-5929
Zhehui Wang https://orcid.org/0000-0001-7826-4063
John Foster https://orcid.org/0000-0001-8369-1828

References

- [1] Locke B R, Sato M, Sunka P, Hoffmann M R and Chang J-S 2006 *Ind. Eng. Chem. Res.* **45** 882–905
- [2] Bruggeman P J et al 2016 Plasma Sources Sci. Technol. 25 053002
- [3] Stancampiano A, Gallingani T, Gherardi M, Machala Z, Maguire P, Colombo V, Pouvesle J-M and Robert E 2019 Appl. Sci. 9 3861
- [4] Sasaki K, Ishigame H and Nishiyama S 2015 Eur. Phys. J. Appl. Phys. 71 20807
- [5] Shirai N, Suga G and Sasaki K 2020 Plasma Sources Sci. Technol. 29 025007
- [6] Bruggeman P, Liu J, Degroote J, Kong M G, Vierendeels J and Leys C 2008 J. Phys. D: Appl. Phys. 41 215201
- [7] Moon D E and Webb M R 2020 J. Anal. At. Spectrom. 35 1859–67
- [8] Kovach Y E, Garcia M C and Foster J E 2019 IEEE Trans. Plasma Sci. 47 3214
- [9] Yang Z, Kovach Y and Foster J 2021 J. Appl. Phys. 129 163303
- [10] Kovach Y E, Wang Z and Foster J E 2021 *Appl. Phys. Lett.* **119** 134102

- [11] Shi Y, Miloshevsky G and Hassanein A 2011 Fusion Eng. Des. **86** 155–62
- [12] Spiel D E 1994 J. Geophys. Res. 99 10289-96
- [13] Deike L 2022 Annu. Rev. Fluid Mech. 54 191-224
- [14] Chen Q, Li J and Li Y 2015 J. Phys. D: Appl. Phys. 48 424005
- [15] Foster J E, Kovach Y E, Lai J and Garcia M C 2020 Plasma Sources Sci. Technol. 29 034004
- [16] Kovach Y E, Garcia M C and Foster J E 2021 Plasma Sources Sci. Technol. 30 015007
- [17] Brown D, Christian W and Hanson R 2022 Tracker video analysis and modeling tool https://physlets.org/tracker/
- [18] Castrejón-Pita A A, Castrejón-Pita J R and Hutchings I M 2012 Phys. Rev. Lett. 108 074506
- [19] Holgate J T, Coppins M and Allen J E 2018 Appl. Phys. Lett. 112 024101
- [20] Rumbach P, Witzke M, Sankaran R M and Go D B 2013 J. Am. Chem. Soc. 135 16264–7
- [21] Hickling A 1971 Electrochemical processes in glow discharge at the gas-solution interface *Modern Aspects of Electrochem*istry No. 6 (Berlin: Springer) pp 329–73

- [22] Witzke M, Rumbach P, Go D B and Sankaran R M 2012 J. Phys. D: Appl. Phys. 45 442001
- [23] Rumbach P, Bartels D M, Sankaran R M and Go D B 2015 *Nat. Commun.* **6** 7248
- [24] Spiel D E 1998 J. Geophys. Res. 103 24907-18
- [25] MacIntyre F 1972 J. Geophys. Res. 77 5211-28
- [26] Kientzler C F, Arons A B, Blanchard D C and Woodcock A 1954 Tellus 6 1–7
- [27] Ghabache E and Séon T 2016 Phys. Rev. Fluids 1 051901
- [28] Nikiforov A Y, Sarani A and Leys C 2011 Plasma Sources Sci. Technol. 20 015014
- [29] Bruggeman P, Cunge G and Sadeghi N 2012 Plasma Sources Sci. Technol. 21 035019
- [30] Xiong Q, Yang Z and Bruggeman P J 2015 J. Phys. D: Appl. Phys. 48 424008
- [31] Laux C O 2002 Radiation and nonequilibrium collisional-radiative models von Karman Inst. Lect. Ser. vol 7 pp 83–121
- [32] Rodero A and García M C 2017 J. Quant. Spectrosc. Radiat. Transfer 198 93–103
- [33] Nikiforov A Y, Leys C, Gonzalez M A and Walsh J L 2015 Plasma Sources Sci. Technol. 24 034001